

Article

Engineering Properties and Environmental Impact of Soil Mixing with Steel Slag Applied in Subgrade

Yangpeng Zhang^{1,2,*}, Tinghui Jiang¹, Shuyang Li¹ and Wensheng Wang^{3,*} ¹ Guangxi Transportation Science and Technology Group Co., Ltd., Nanning 530007, China² School of Traffic & Transportation Engineering, Changsha University of Science & Technology, Changsha 410114, China³ College of Transportation, Jilin University, Changchun 130025, China

* Correspondence: zyp_engineering@outlook.com (Y.Z.); wangws@jlu.edu.cn (W.W.)

Abstract: The purpose of this study was to evaluate the feasibility of the large-scale application of steel slag (SL) in subgrade. Subgrade materials with three kinds of SL proportions were first prepared. Then, a compaction test, liquid-plastic limit combined-measurement test, and a California bearing ratio (CBR) test were applied to determine the best proportion between SL and intact soil (S), i.e., SL/S. Subsequently, static and dynamic tests and a volume stability test were carried out for soil mixed with SL at the optimum proportion (SSL). In addition, a composition analysis of infiltration fluid and a permeability test of SSL were performed. The test results showed that compared to S, the physical properties of SSL were significantly improved, especially the liquid-plastic limit, as well as the soil water stability. The optimum proportion of SL was determined as 50% of soil by mass. At the optimum proportion, SSL had the highest CBR value of 60%, which had both economic and engineering compaction performance, leading to a large-scale utilization rate of SL. The static and dynamic characteristics showed that the addition of SL would greatly improve the shear strength and dynamic modulus of soil, mainly expressed as the increase of internal friction angle. The volume stability of SSL could also meet the requirements of the Chinese specification. After adding 2% cement, the strength and stability of SSL was further improved. In addition, the environmental impact test proved that the infiltration liquid did not pollute surface water nor underground secondary water. Although the permeability coefficient of SSL with the optimum proportion of 50% was higher than that of pure soil, it still belonged to the normal value of clay and silty clay, and good impermeability would ensure the controllability of potential trace elements. Based on the test results of mechanical properties and environmental impact, SSL proved to have the potential for green road material engineering properties. This study proposes a reliable and practical method to promote the utilization of steel slag.

Keywords: steel slag; subgrade material; physical property; mechanical property and stability; environmental impact



Citation: Zhang, Y.; Jiang, T.; Li, S.; Wang, W. Engineering Properties and Environmental Impact of Soil Mixing with Steel Slag Applied in Subgrade. *Appl. Sci.* **2023**, *13*, 1574. <https://doi.org/10.3390/app13031574>

Academic Editor: Luis Picado Santos

Received: 27 November 2022

Revised: 15 January 2023

Accepted: 17 January 2023

Published: 26 January 2023



Copyright: © 2023 by the authors. Licensee MDPI, Basel, Switzerland. This article is an open access article distributed under the terms and conditions of the Creative Commons Attribution (CC BY) license (<https://creativecommons.org/licenses/by/4.0/>).

1. Introduction

Steel slag (SL) is a bulk industrial by-product in the steel-making process. In 2012, the annual production of SL in China was 90 million tons, and exceeded 100 million tons in 2020, ranking first in the world. At present, China's accumulated SL volume has exceeded 4 billion tons, but its utilization rate is less than 30% [1–3]. The environmental burden caused by SL piling is becoming more and more serious. The main uses of SL can be summarized as steel-making recycling, sintering material, iron dephosphorization, road and water construction, production of cement, concrete, and other construction materials, water pollution treatment, carbon sequestration and desulphurization, agriculture, and nine other uses [4–6], among which road construction is the most important application for SL, shown in Figure 1.

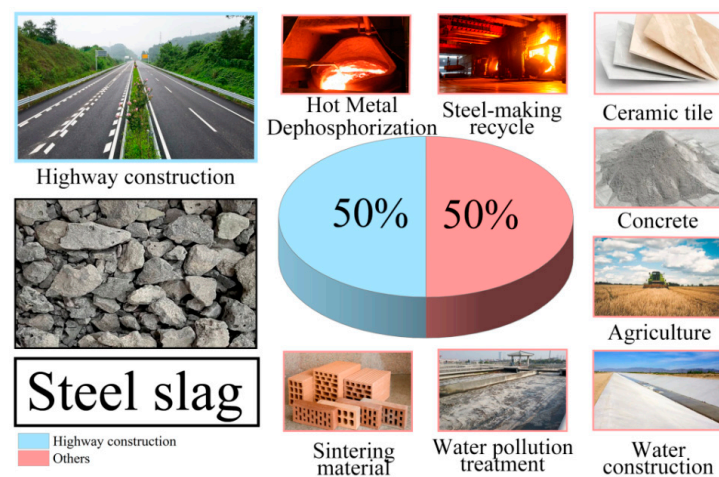


Figure 1. The main uses of SL.

Due to its compressive strength and wear resistance, it has been recognized that SL can be used as an aggregate. In 1974, Canada constructed a test road with SL for the 401 expressway, and its excellent anti-slip properties were noticeable after four years. In the 1980s, Japan began combining asphalt pavement with SL to improve skid and wear resistance. Subsequently, SL aggregates have been widely applied in the US, Germany, Singapore and other countries [7]. In 2009, SL was used instead of basalt to pave the surface pavement layer in Beijing, and the first all SL municipal road was completed in Taiyuan, Shanxi in 2015 [8]. Asphalt mixed with SL can serve as a partial replacement for aggregates and significantly improve physical and mechanical properties and fatigue resistance [9–13]. More recently, waste/recycled materials have gradually been used for stabilizing subgrades. Yaghoubi et al. [14] studied the utilization of environmentally clean recycled aggregates, such as recycled glass, for improving subgrades with problematic soils. Mirzababaei et al. [15] carried out a comprehensive investigation on the utilization of carpet waste fibers in the reinforcement of clay soils. These relevant studies provided reference for the utilization of SL.

Scholars have extensively attempted to use SL in road subgrade and subbase [16–19]. Li et al. [16] performed dry shrinkage and temperature shrinkage tests on cement-stabilized steel slag by using SL instead of crushed stone, and found that a reasonable adjustment of SL gradation could effectively reduce the dry shrinkage and temperature shrinkage. Liu et al. [17] examined the effect of different SL dosing on the mechanical properties of cement-stabilized crushed stone subgrade. The strength and stiffness of cement-stabilized aggregates were optimal with an SL of 50%. Li et al. [18] also obtained the best mechanical properties and durability of water-stabilized subgrade material when SL was mixed at 50%. Gao et al. [19] applied SL in the construction of highway roadbeds, and the compaction, surface flatness and compressive strength of water-stabilized SL aggregate subgrade met road construction requirements. Therefore, another major application for SL is road base construction, with the prospects even more promising. The high strength, wear resistance and granular properties of the friction strength and mechanical stability of SL can effectively improve the load-bearing capacity and stability of road foundations [20]. The main structure of SL is similar to the composition of cement, so it is also used as a cementitious material instead of cement and lime, for reinforcement and improvement of poor soil properties [21–23]. The application of SL for road bases in China began in the 1960s, and the flat-furnace SL combined with soil was used as a road-base material, which proved that SL can be used for subgrade filling [24–26]. Compared to its application in pavement, the application of SL in the subgrade will be much larger, and the requirements for the homogeneity and index of raw materials are relatively lenient. However, the potential swelling hazards caused by active substances in SL cannot be ignored. The application of steel slag in road-base engineering in China is still used in small-scale blending, mostly

together with other by-products. There are few cases of large-scale SL use, and the research on the mechanical characteristics and stability control of SL as a subgrade filler is not yet perfect. In addition, the potential environmental pollution of SL is of great importance because it generates several by-products due to the use of a number of agents during its production process. When SL is used as subgrade fill, the metal ions, trace elements and acidity within the infiltration fluid produced from surface water or groundwater can potentially contaminate surrounding land and water resources.

Based on the above background, this paper presents a study on the application of subgrade with large doses of SL as typical fills in Guangxi, China, with the aim to obtain a subgrade fill that is reliable and environmentally friendly. Through compaction, liquid-plastic limit and CBR tests, the optimum proportion of soil mixing with SL (SSL) was determined, and its dynamic characteristics were investigated through static and dynamic tests. Finally, the environmental impact of SSL in the subgrade was evaluated. The test results, mechanical properties, and environmental analyses of the SSL subgrade in this study aim to promote the application of waste materials to support sustainable development, while achieving improved performance of subgrade materials.

2. Materials and Experimental Methods

2.1. Raw Materials

2.1.1. Soil

The soil samples in this study were collected from two sections of an expressway construction site in Qinzhou City, Guangxi, named soil sample 1 (S1) and soil sample 2 (S2), respectively. The maximum dry density of S1 and S2 were 1.92 g/cm^3 and 1.95 g/cm^3 , respectively, and the corresponding maximum water content were 10.4% and 12.4%, respectively. The liquid limit of S1 was 43.7%, and its plasticity index was 12.2%. The liquid limit of S2 is 59.6%, and its plasticity index was 31.9%. Referring to T0115-1993 in the Chinese specification (JTG 3430-2020), according to this method of soil classification of the plastic diagram, S1 was silty clay and S2 belongs to high liquid limit clay. The grading curves of S1 and S2 are shown in Figure 2. For S1, the coefficient of uniformity (Cu) and coefficient of curvature (Cc) were 2.9 and 0.8, respectively, and the Cu and Cc of S2 were 6.3 and 72.3, respectively, which were poor gradings. The XRD analysis results for S1 and S2 showed that there were more quartz components, and S2 also contained some components of CaCO_3 , as shown in Figure 3a,b.

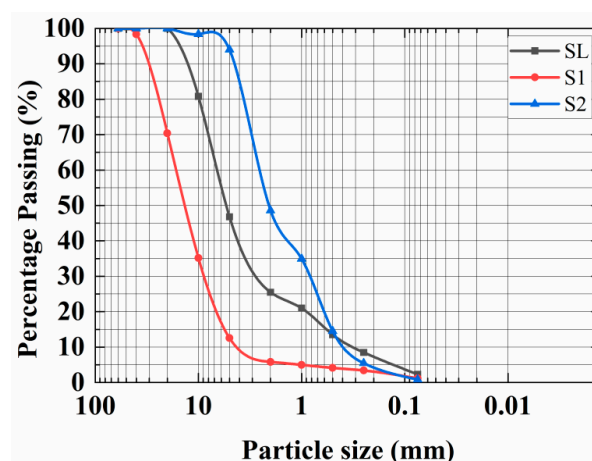


Figure 2. The grading curves of soil and SL used in this study.

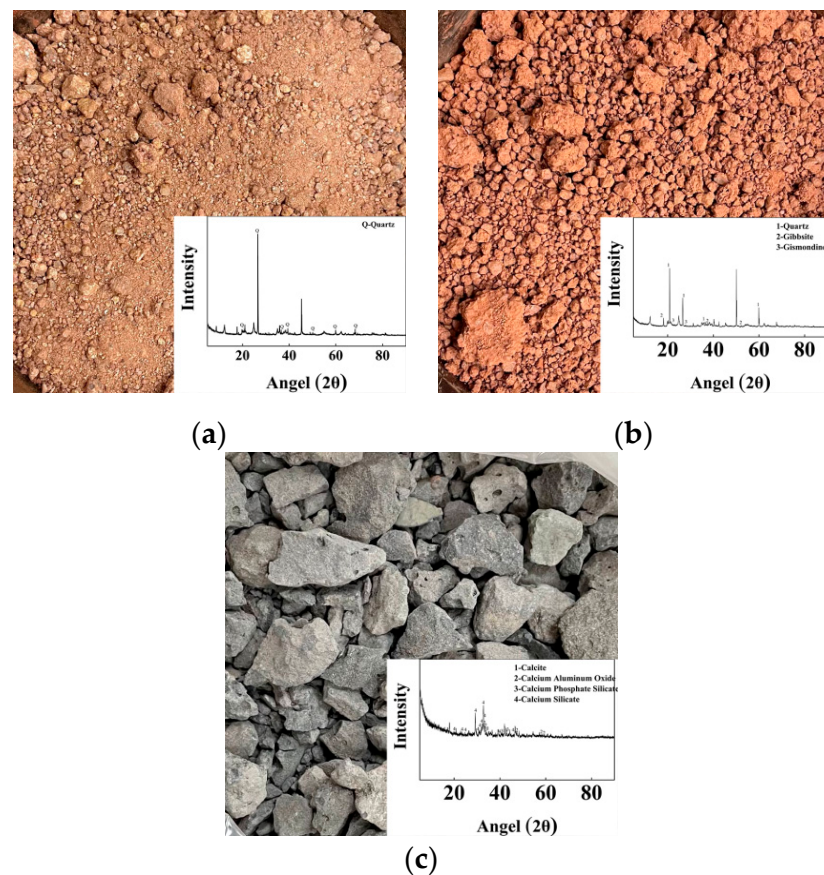


Figure 3. The experimental raw materials and XRD analysis results: (a) S1; (b) S2; (c) SL.

2.1.2. Steel Slag

The steel slag used was the hot, stuffy steel slag taken from an iron and steel plant in Guangxi, which was processed by magnetic separation during production, as shown in Figure 3c. The natural water content of SL was 0.32~0.62%, and its particle specific gravity was 3.36. The grading curve of SL is shown in Figure 2. The corresponding C_u and C_c were 14 and 1.9, respectively, so the SL used belonged to a good grading. The XRD analysis result showed that the SL used was mainly composed of calcium carbonate, calcium alumina, calcium phosphate silicate and calcium silicate, as shown in Figure 3c. The SL used in this test was aged for six months. After immersion, the volume expansion rate was 1.51%, and the pulverization rate was 4.8%, meeting the requirements of the Chinese specification (GB/T 25824-2010).

2.1.3. Specimen Preparation

In this study, a set of test soil with different proportions of soil and SL were prepared to carry out the relevant experiments. In order to improve the utilization rate of SL and give full play to the strength advantage of SL, soil specimens mixed with SL at 30%, 50% and 70% of soil by mass were selected. Compared with the existing research, the above content of SL in this study was greatly increased [20,25]. Before the laboratory tests, soil and SL samples were dried at a temperature of 110 ± 5 °C for 8 h and then cooled at room temperature. The SSL specimens were manually prepared according to the target mix proportion and water content during the whole preparation process. According to the experimental method of Chinese specification (JTG 3430-2020), the SSL specimens with the dimension of $\Phi 152$ mm \times 120 mm and $\Phi 39.1$ mm \times 80 mm were used for compaction, liquid plastic limit, CBR, static and dynamic tests, etc. Some test specimens had to be cured for 7 d after specimen preparation. The specimens for the environmental impact assessment test were taken from specimens that failed the mechanical tests.

2.2. Experimental Methods

2.2.1. Determination of Optimum Proportion (SL/S) between SL and Intact Soil

The proportion of improved soil was determined by its compaction performance, boundary water content characteristics and bearing capacity characteristics, which were examined through a compaction test, liquid-plastic limit combined measurement test and California bearing ratio (CBR) test.

(1) Compaction test

According to the Chinese specification (JTG 3430-2020), the maximum dry density and maximum water content can be determined by using the method of T 0131-2019. For each mixed proportion, five samples with an interval of 2% water content were first prepared in which each specimen was made by 98 compaction times. After compaction and demolding, the mass and water content of the specimens were measured, and then the maximum dry density curve under different water contents was determined.

(2) Liquid-plastic limit combined measurement test

According to the Chinese specification (JTG 3430-2020), the liquid-plastic limit combined measurement test in T 0118-2007 was used. Before the test, the samples were passed through a 0.5 mm sieve to prepare three specimens, in which the water contents were controlled at the liquid limit (point a), slightly greater than the plastic limit (point c) and the intermediate state (point b), respectively. A cone with a mass of 100 g was used in the test, where the cone penetration depth of point a was (20 ± 0.2) mm, and the cone penetration depth of point c was less than 5 mm. Based on the test results, the cone penetration depth versus water content referring to points a, b, and c could be drawn on double logarithmic coordinates. Points (a, b and c) had to be in a straight line. Otherwise, they had to be adjusted to a hyperbola h_p-w_L to obtain the corrected direct line (ad). The liquid limit corresponded to the penetration depth of 20 mm, and the plastic limit was determined according to the double curve specified in the specification. The process is briefly presented in Figure 4.

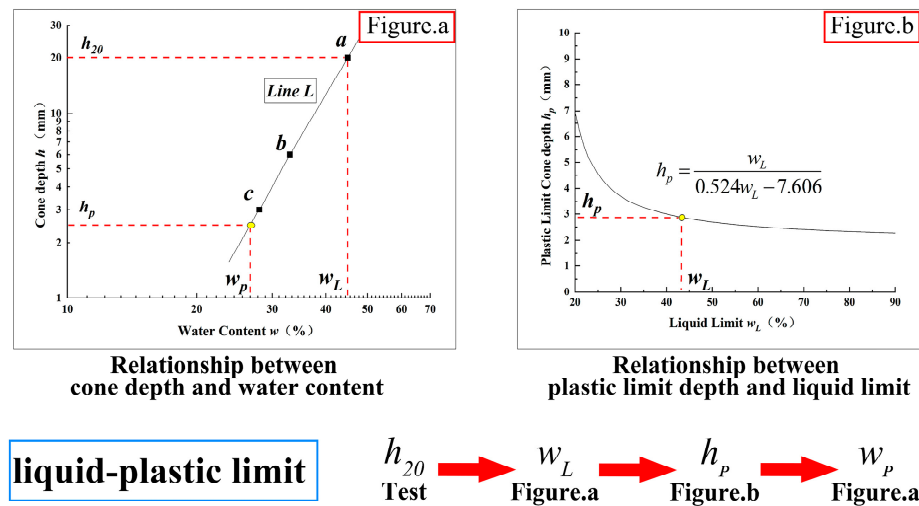


Figure 4. The process of determining the liquid and plastic limit of test soils.

(3) CBR test

The specimens were prepared by the same forming method as the compaction test. For each proportion, the specimens were molded in the state of maximum dry density and optimum water content. After immersion for 96 h, the immersion height and water absorption mass were measured, and then a CXY-128B pavement material strength tester was used for testing and automatically recording the rod penetration depth and corresponding data. Thus, the corresponding testing values when penetrated at 2.5 mm and 5.0 mm were obtained.

2.2.2. Mechanical Properties and Deformation Stability of Soils

In order to evaluate the mechanical properties and stability of SSL, static and dynamic tests were carried out and the volume stability test was also conducted for the deformation stability of SSL. In addition, considering that a small amount of cement has been used to improve the strength and stability of soil in many studies [27–29], this paper also carried out the laboratory test of SSL incorporating 2% cement (i.e., SSLC).

(1) Static triaxial test

The static triaxial test is usually adopted to evaluate internal friction and cohesion. The shear strength values of soil, SSL, and SSLC could be measured by the static triaxial test. Based on the optimal water content and maximum dry density, the specimens with a diameter of 39.1 mm and a height of 80 mm were prepared by simulating the reality with the compactness of 96%. In this study, the TKA-TTS-1 full-automatic triaxial apparatus shown in Figure 5a was selected, and the confining pressure was set as 50, 100, and 150 kPa, with a longitudinal loading speed of 0.02 mm/min. When the failure or longitudinal deformation reached 5%, the static triaxial test would stop, and the stress-strain curve could be drawn. Based on the limit equilibrium method, the cohesion (c) and friction angle (φ) could be solved.

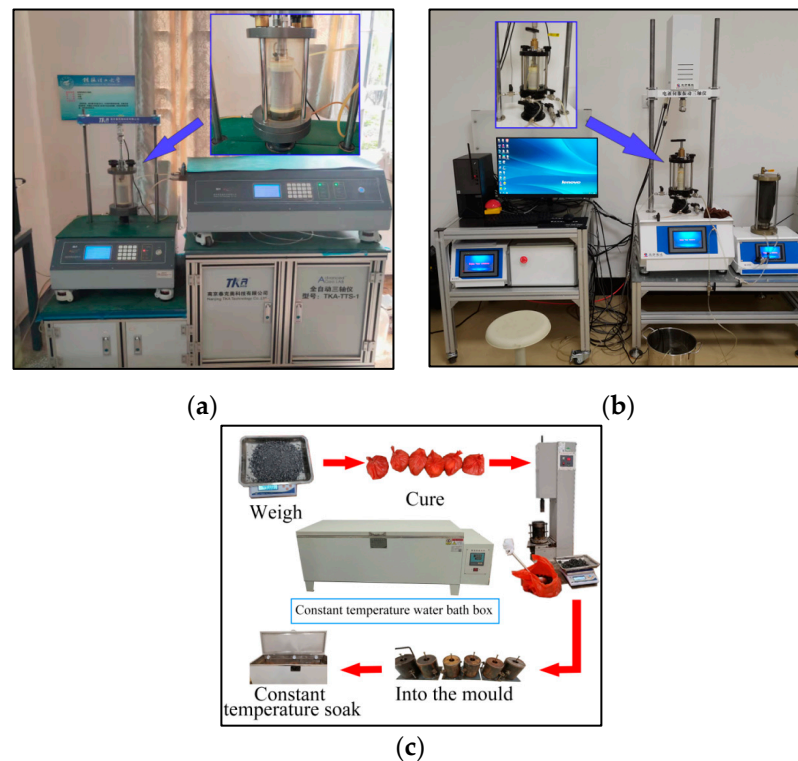


Figure 5. The experimental procedure of mechanical properties and deformation stability: (a) static triaxial test; (b) dynamic modulus test; (c) volume stability test.

(2) Dynamic modulus test

In this study, the LFTD1821 dynamic triaxial testing machine was used for the dynamic modulus test according to the Chinese specification (GB/T 50123-2019), as shown in Figure 5b. The dynamic modulus test is commonly used to evaluate the dynamic characteristics of soil materials [30,31]. The specimen size was the same as that of the static triaxial test, and the specimens were also prepared with a compactness of 96%. The consolidation was completed at the coefficient 1.1. Sinusoidal cyclic loading with a frequency of 1 Hz at the confining pressure of 100 kPa was applied. The selected parameters frequency and confining pressure are the most commonly used, and closest to the engineering situation. In order to obtain the deformation response of the specimen under different dynamic pressures, the longitudinal deviatoric stress was continuously increased from small to

large (i.e., varying from 5 kPa to 350 kPa, at the amplitude of 5~50 kPa). Ten cycles were performed for each deviatoric stress state. The stress-strain curve data in the last cycle was extracted for calculation of the dynamic modulus.

(3) Volume stability test

For SL, the volume stability is the most critical factor to determine the engineering application. According to the requirements of the Chinese specification (GB/T24175-2009), the water immersion expansion rate test was carried out to measure the volume change of SL, SSL, and SSLC after immersion. The soil specimens were prepared according to the particle size requirements and formed by heavy compaction. Referring to the immersion conditions of the CBR test, the specimens were put into a thermostatic water bath and the data recorded. The water temperature was then kept at 90 ± 3 °C for 6 h and afterwards heating stopped. Data after 18 h (the next day) was recorded before heating. The above process was repeated and the final data was recorded after 10 d, in which the volume change during the process could be obtained. The details of the volume stability test are shown in Figure 5c.

2.2.3. Environmental Impact Assessment Methods

(1) Composition analysis of infiltration fluid

The SL used for subgrade soil filling has low activity and fewer adverse reactions and emissions; however, the biggest hidden danger is the potential pollution of infiltration fluid in the subgrade. According to the Chinese specification (GB 5085.3-2007), the composition analysis of infiltration fluid was carried out to measure copper, zinc, cadmium, lead, chromium, hexavalent chromium, mercury, barium, nickel, arsenic and selenium [32]. In accordance with the Chinese specification (HJ/T 298), after the samples were treated, the contents of relevant elements were measured using a GGX-810 atomic absorption spectrophotometer, an AFS-8520 atomic fluorescence spectrophotometer and a T6 ultraviolet visible spectrophotometer, respectively. Table 1 lists the specific determination methods and standards.

Table 1. The specific determination standards and instruments in the composition analysis of infiltration fluid.

No.	Element	Standard	Instrument	Detection limit
1	Cadmium			0.9 µg/L
2	Lead	HJ 787-2016	GGX-810	0.6 µg/L
3	Zinc	HJ 786-2016	GGX-810	0.06 mg/L
4	Arsenic			0.10 µg/L
5	Mercury	HJ 702-2014	AFS-8520	0.02 µg/L
6	Selenium			0.10 µg/L
7	Copper			0.02 mg/L
8	Nickel	HJ 751-2015	GGX-810	0.03 mg/L
9	Total chromium	HJ 749-2015	GGX-810	0.03 mg/L
10	Hexavalent chromium	GB/T 15555.4-1995	T6	0.004 mg/L
11	Barium	GB 5085.3-2007	GGX-810	0.1 mg/L

(2) Permeability test

Permeability evaluation is an important indicator for the application of industrial solid waste in the subgrade. According to the Chinese specification, the permeability test was carried out by using T 0130-2007. The test water was degassed with the boiling method before the test, and the specimens were prepared using a circular knife with an inner diameter of 61.8 mm and a height of 40 mm. Considering the actual engineering situation, the variable head permeability test was conducted on the specimens with the compactness of 96% at the room temperature of 20 °C.

3. Results and Discussion

3.1. Determination of Optimum Proportion (SL/S) between SL and Intact Soil

3.1.1. Compaction Test

Figure 6 shows the compaction curves of intact soil (S) and SSL with various proportions of SL/S for two kinds of soil samples (i.e., S1 and S2). From Figure 6, the maximum dry density of SSL with S1 was 2.14–2.45 g/cm³, and the maximum dry density of SSL with S2 was 2.10–2.35 g/cm³, displaying an increasing trend with increasing SL content (i.e., from 30% to 70%). The optimum water content of SSL with S1 was 9.9~10.9%, and the optimum water content of SSL with S2 was 8.7~10.2%, showing a changing trend opposite to the maximum dry density. This phenomenon was closely related to the physical properties of SL. The specific gravity density of SL was 3.36, which was much higher than 2.68 and 2.64 for S1 and S2, respectively. Therefore, the optimum dry density of SSL was higher than that of intact soil (S). At the same time, as a low cohesion material, the content of viscous particles in SL was lower, so the optimum water content decreased.

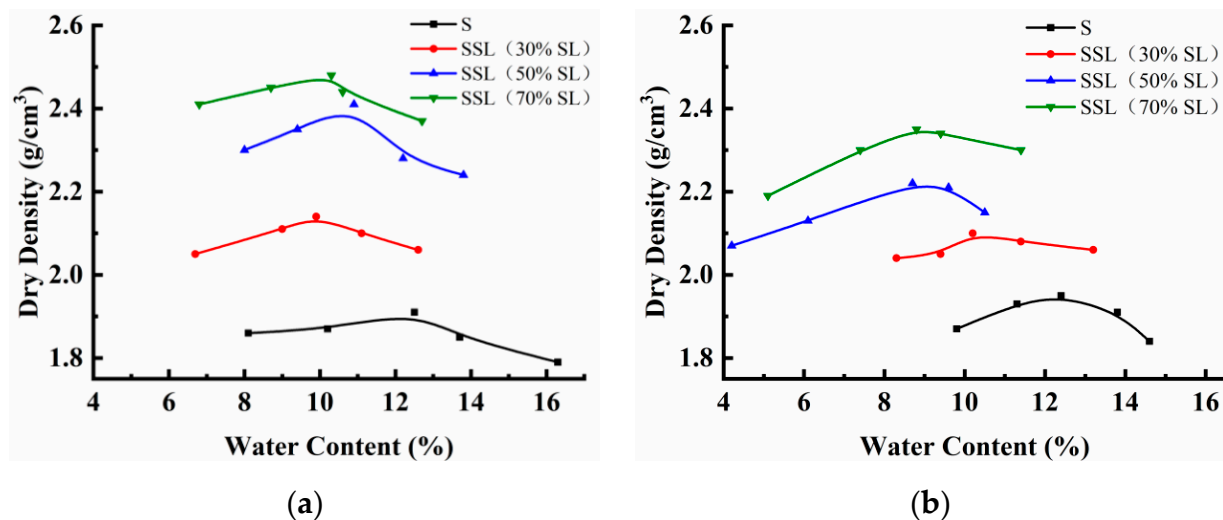


Figure 6. The compaction test results: (a) compaction curves of specimens from S1; (b) compaction curves of specimens from S2.

Greater compaction work is required during construction, especially for high-strength SL. A subgrade filler with higher SL content requires more energy consumption. Therefore, selecting the optimum proportion of SSL is of great significance for engineering applications.

3.1.2. Liquid-Plastic Limit Combined Measurement Test

Table 2 shows the results of the Atterberg limits test for two kinds of soil samples (i.e., S1 and S2) mixed with SL. It was observed that with the addition of SL, the liquid-plastic limit of the test soil specimen decreased. Due to the greater drop in the liquid limit, the plasticity index also decreased. This phenomenon can also be attributed to the reduction of the clay particle content. Furthermore, SL can contain a small number of active components, and the potential chemical reaction can also lead to a change in the Atterberg limit value; however, this was ignored because the SL used in this study had low activity.

Table 2. Limit water content of soil mixed with different SL contents.

Sample Type	SL Content (%)	Liquid Limit Water Content (%)	Plastic Limit Water Content (%)	Plasticity Index
S1	0	43.7	31.5	12.2
	30	38.1	26.5	11.6
	50	36.0	25.2	10.8
	70	25.2	19.1	6.1
S2	0	59.6	27.7	31.9
	30	43.7	26.7	17.0
	50	34.4	24.9	9.4
	70	29.3	20.0	9.3

In this study, S1 was silty clay and S2 contained high liquid limit clay. At 0% SL content, the liquid limit was 43.7%~59.6%, and the plasticity index 12.2% and 31.9%. The high plasticity index means that the water sensitivity was low, but the water stability of soil with a higher liquid limit was poor, which could also lead to poor compactness of subgrade filler. Compaction during the engineering construction could be difficult, resulting in some problems with later shrinkage and deformation. Therefore, the addition of SL had an obvious improvement effect on the liquid and plastic limits of S1 and S2. With the increase in the amount of SL, the plasticity index of the test soils S1 and S2 decreased, as shown in Figure 7.

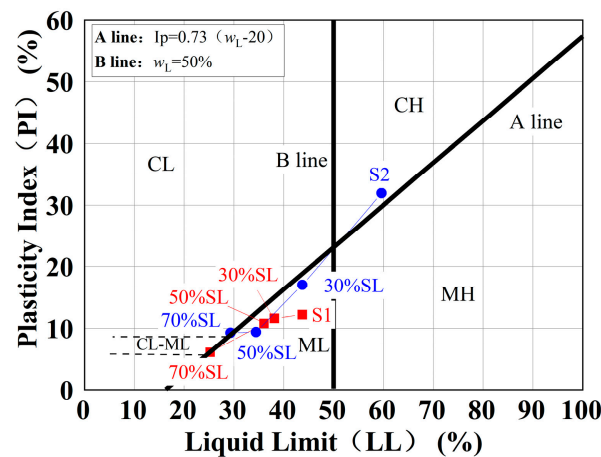


Figure 7. The plastic zones of soil specimens in this study.

3.1.3. CBR Test

The CBR values of the test soils (S1 and S2) mixed with SL after 96 h-immersion are shown in Figure 8. From Figure 8, it can be seen that the CBR values of the test soil specimens were 15%~60%. According to the requirements of the Chinese specifications on subgrade design, the roadbed on expressways and Class I roads is greater than 8%, that on Class II roads is 6%, and that on Class III and IV roads is 5%. The CBR values of the test soil specimens (S1 and S2) before improvement were 5% and 22%, respectively, which have a certain bearing capacity, but the water stability was poor. After adding SL, the CBR values of the test soil improved significantly, and the water absorption gradually reduced, which ensures the strength and stability of the test soil used as roadbed for high-grade roads, and the embankment and subgrade could also meet requirements. A higher CBR value means a higher bearing capacity. Therefore, soil mixed at a proportion of 50% SL was the best choice.

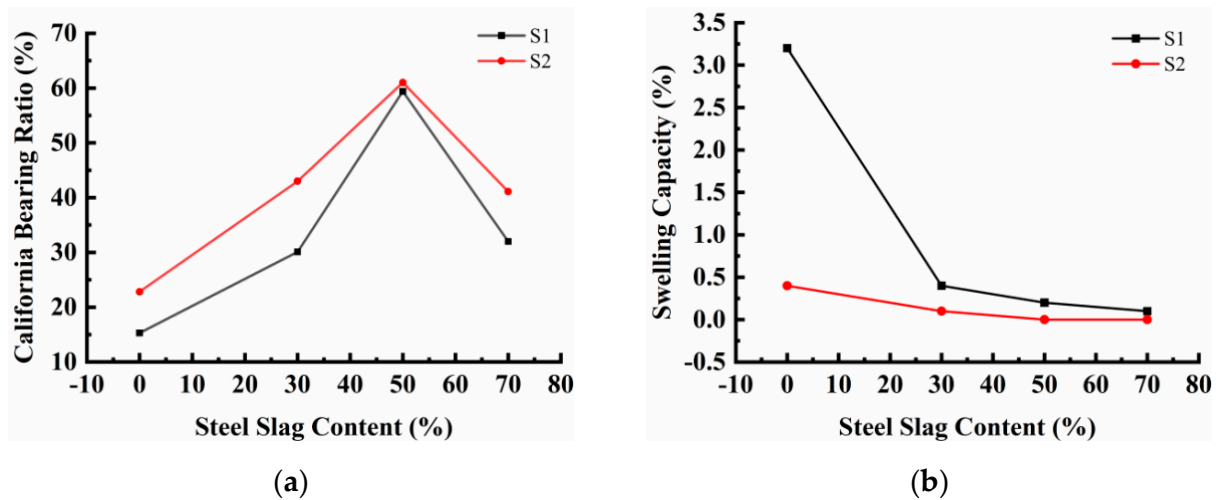


Figure 8. The CBR test results: (a) CBR values; (b) swelling capacity.

The CBR of the test soil mainly came from materials and structures, and there was little hydration of active substances. With the addition of SL, the CBR of the improved soil SSL first increased and then decreased due to its structural composition. The addition of SL makes the soil and SL form a reliable and stable structure. However, with excessive SL, this balance is broken, leading to a decrease in strength and the “inflection point”, as shown in Figure 8a. In addition, it was observed that with the increase of compactness, the CBR value also increased, and the water absorption and expansibility decreased, making the subgrade structure more stable. From Figure 8b, it can be seen that the swelling capacity decreased with increasing steel slag content.

To summarize, the compaction characteristics, Atterberg limit value and CBR values showed that the improved soil mixed with SL (i.e., SSL) performed well, especially the SSL with 50% SL which had the highest CBR strength, and can solve the potential stability problems caused by the high liquid limit of intact soil. Considering the economic and compaction characteristics, the improved soil mixed with 50% SL also had the characteristics of a high utilization rate of SL, which was selected for the following study.

3.2. Mechanical Properties and Deformation Stability of Soils

3.2.1. Static Triaxial Test

The stress-strain curves of intact soil (S), SSL and SSLC under the confining pressure of 50, 100, and 200 MPa are plotted in Figure 9. As shown in Figure 9, with increased deformation, longitudinal stress also gradually increased, while the slope of the stress-strain curve gradually decreased with increased deformation. When the stress-strain curve reached the peak value, it remained unchanged or decreased. The peak strain in the stress-strain curve was selected as the failure limit. The failure strain values of the test soil specimens were between 2.5% and 4%, which conforms to the normal failure law of soil. Figure 9 shows that the failure deviatoric stress corresponding to the failure strain was: SSLC > SSL > S.

Based on the Lambe plane (s,t) method, the cohesion (c) and friction angle (φ) of the test soil were calculated, as shown in Figure 10 and Table 3. The cohesion and friction angle of intact soil were 42.24 kPa and 25.27°, respectively, consistent with previous research [33]. The contribution of cohesion to shear strength was higher, especially under low stress. With the addition of SL, the shear strength of the soil improved as a whole. Under the same stress condition, the shear strength of the improved soil significantly increased by 1.75%~2.05%, which was mainly attributed to the increase of cohesion and friction angle caused by the addition of SL. Compared with the intact soil, the cohesion and friction angle of SSL increased by 20% and 66%, respectively, especially under high stress. The addition

of cement further improved SSL’s strength, cohesion and friction angle, especially cohesion which was 1.5 times higher than that of SSL alone, highlighting the role of cement.

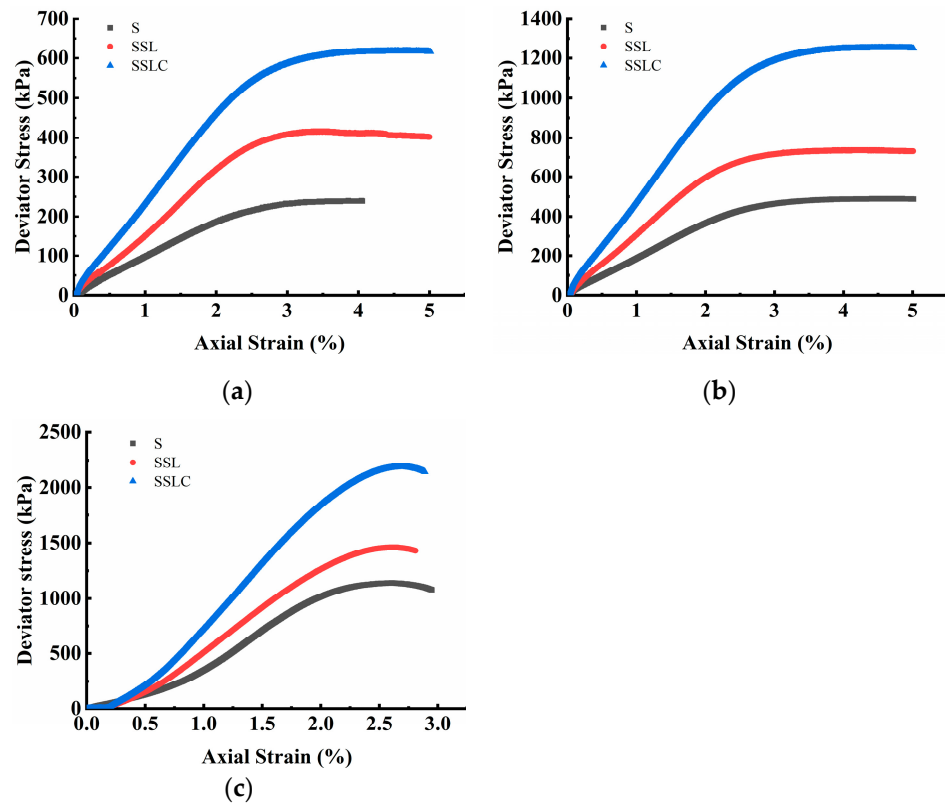


Figure 9. The stress-strain curves at different confining pressures: (a) 50 MPa; (b) 100 MPa; (c) 200 MPa.

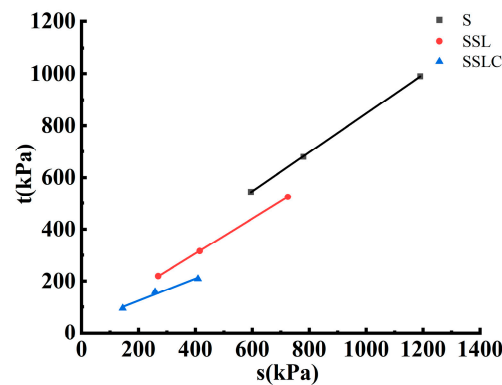


Figure 10. The relationship curve of (s,t).

Table 3. Strength parameters of test soil.

Strength Parameters	S2	SSL	SSLC
Cohesion (c) (kPa)	42.24	50.77	128.06
friction angle (φ) ($^{\circ}$)	25.27	42.14	48.5

The strength parameters of the test soil were used to estimate the strength and stability of the subgrade for practical engineering. The results showed that SSL performed well and improved the intact soil. The addition of cement further improved the strength of SSL. For this reason, cement, lime, etc. are often used as soil reinforcements to improve poor soil.

The strength of the improved soil even meet the requirements of a road base, which would be another road application for SSL.

3.2.2. Dynamic Modulus Test

Figure 11a shows the dynamic stress-strain curves of intact soil (S), SSL and SSLC. It can be seen that the stress increased with increasing strain, and the slope of these curves gradually decreased, showing that the dynamic modulus decreased. Among the test soil specimens, the dynamic modulus of SSLC was the largest, followed by SSL, and finally S. The dynamic modulus test results were consistent with the above static triaxial strength and bearing capacity results. The point line diagram of the dynamic modulus curve was obtained using the dynamic stress-strain curves, as shown in Figure 11b. Unlike the trend seen for the stress-strain curve, the dynamic modulus decreased with increased axial strain, mainly because increased deformation leads to plastic reinforcement and elastic attenuation, so dynamic modulus decreases.

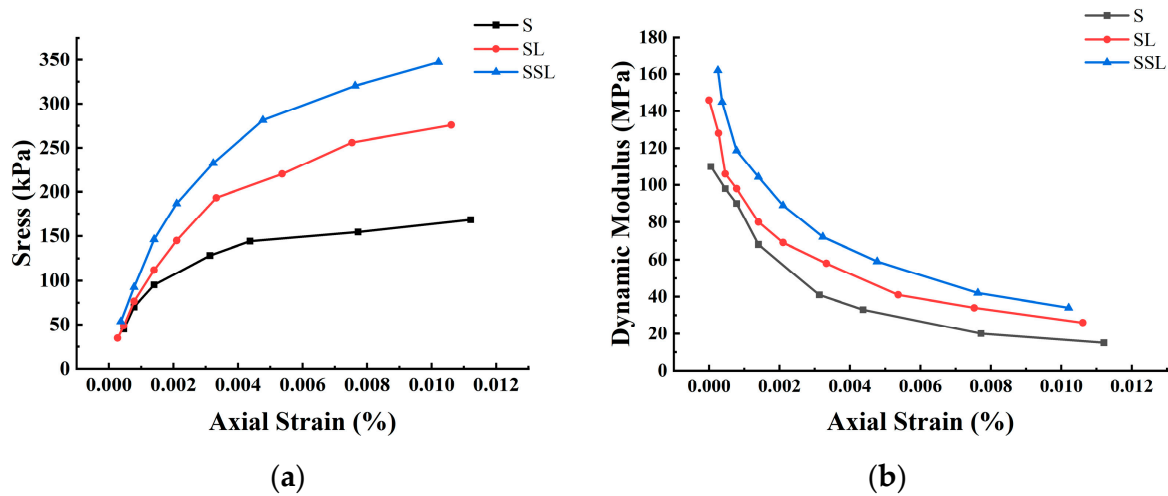


Figure 11. The dynamic modulus test results: (a) dynamic stress-strain curve; (b) dynamic re-bound modulus curve.

Dynamic modulus is an important parameter to evaluate the subgrade deformation in construction. In order to better analyze the dynamic modulus test results, Equation (2) converted from Equation (1) (Hardin-Drnevich model) was used to fit the curve of dynamic modulus versus strain:

$$\sigma_d = \frac{\epsilon_d}{A + B\epsilon_d} \tag{1}$$

$$E_d = \frac{1}{A\epsilon_d + B} \tag{2}$$

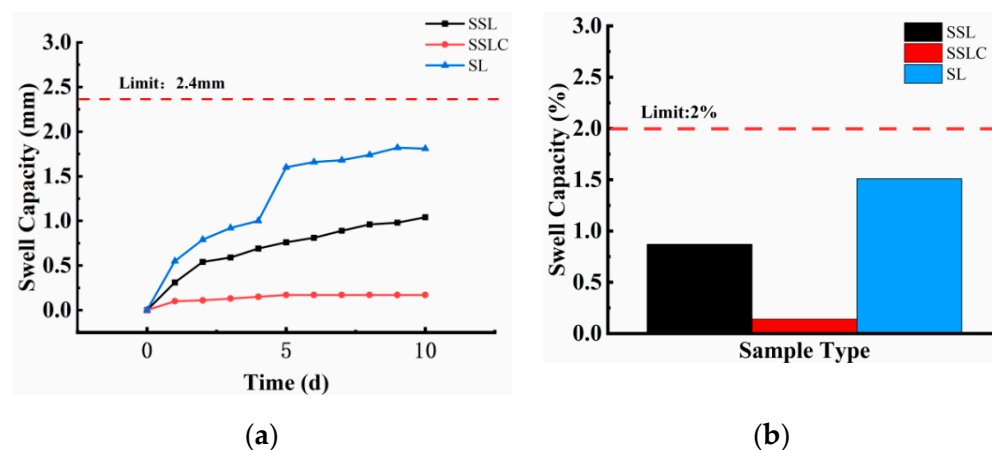
in which A and B are fitting parameters. It is worth noting that when the longitudinal strain (ϵ_d) is close to 0, the dynamic modulus E_d is equal to $1/B$, which is usually defined as the maximum dynamic modulus E_{dmax} . According to Equation (1), the values of A , B and E_{dmax} of the test soil are calculated and listed in Table 4. From Table 4, the parameters A and B of intact soil were the highest, and A and B of SSLC were the lowest. The maximum dynamic moduli of the test soil (S, SSL and SSLC) were 118.20 MPa, 140.85 MPa, and 255.75 MPa, respectively, where the intact soil was the lowest, SSL was intermediate, and SSLC was the highest. These results showed the good dynamic modulus characteristics of the improved soils with SL and cement, including SSL and SSLC.

Table 4. The fitting parameters of dynamic modulus.

Types	Parameters			
	A	B	R ²	E _{max} (MPa)
S	4.5394	0.00846	97.89	118.20
SSL	3.4846	0.00710	98.48	140.85
SSLC	1.6921	0.00391	98.74	255.75

3.2.3. Volume Stability Test

The volume stability test results of SL, SSL, and SSLC are shown in Figure 12. For SL, SSL and SSLC, the water immersion expansion rates were 1.51%, 0.87% and 0.14%, which meet the requirements of less than 2% in the Chinese specification (GB/T 24175-2009), suggesting they all have good volume stability. By comparison, it can be seen that the volume expansion rate of SSL was 42% lower than that of SL, and the volume expansion rate of SSLC was 91% lower than that of SL. Therefore, it was obvious that the reduction of the volume expansion rate led to a good stability control effect. For practical engineering applications, SL with a shorter aging time or slightly greater expansibility can be reduced by adding intact soil and cement to improve its volume stability.

**Figure 12.** The volume stability test results: (a) volume expansion curve; (b) final volume expansion rate.

3.3. Environmental Impact Assessment Methods

3.3.1. Composition Analysis of Infiltration Fluid

As a concomitant of steelmaking, SL contains a variety of metal elements, leading to some concerns about whether its infiltration fluid will pollute surrounding soil and groundwater. An environmental assessment of SL thus contributes to encouraging the use of SL in China. This section aims to evaluate the influence of infiltration fluid on nearby surface water and groundwater after the subgrade is covered with water. The composition analysis results of infiltration fluid for these test soils are listed in Table 5. From the 11 trace elements shown in Table 5, for SL, the contents of arsenic, selenium, and hexavalent chromium were 0.62 $\mu\text{g/L}$, 0.54 $\mu\text{g/L}$ and 0.009 mg/L , respectively, and the contents of other trace elements were lower than the detection limits. When the soil was mixed with cement (i.e., SSLC samples), the concentrations of these three trace elements decreased by 0.08 $\mu\text{g/L}$, 0.07 $\mu\text{g/L}$ and 0.001 mg/L , which was mainly caused by the reduction of SL content in the improved soil. It is worth noting that all trace elements in SSLC were lower than the detection limits, reflecting the consolidation effect of cement on trace elements. However, the test results were very vulnerable to the influence of material homogeneity. Uneven mixing of cement may cause degradation of the solidification effect of trace elements, but this positive effect cannot be ignored.

Table 5. The composition analysis results of infiltration fluid.

Element	Samples			Surface Water	Ground Water			Detection Limit
	SL	SSL	SSLC	Class I	Class I	Class II	Class III	
Cadmium	<0.9	<0.9	<0.9	1	0.1	1	5	0.9 µg/L
Lead	<0.6	<0.6	<0.6	10	5	5	10	0.6 µg/L
Zinc	<0.05	<0.05	<0.05	0.05	0.05	0.5	1	0.06 mg/L
Arsenic	<0.10	0.62	0.54	50	1	1	10	0.10 µg/L
Mercury	<0.02	<0.02	<0.02	0.05	0.1	0.1	1	0.02 µg/L
Selenium	<0.10	0.54	0.46	10	10	10	10	0.10 µg/L
Copper	<0.01	<0.01	<0.01	0.01	0.01	0.05	1	0.02 mg/L
Nickel	<0.03	<0.03	<0.03	-	0.002	0.002	0.02	0.03 mg/L
Total chromium	<0.03	<0.03	<0.03	0.01	0.005	0.01	0.05	0.03 mg/L
Hexavalent chromium	<0.004	0.009	0.008	0.01	0.005	0.01	0.05	0.004 mg/L
Barium	<0.1	<0.1	<0.1	0.7	0.01	0.1	0.7	0.1 mg/L

According to the test results in Table 5, all trace elements in the test soils could meet the class I standard of surface water (GB 3838-2022), indicating that the infiltration fluid of subgrade soil mixed with SL meets the environmental requirements. The addition of SL had no impact on the use of common domestic water for drinking and bathing. The standard for groundwater is strict, and the requirements for barium, cadmium, chromium, and nickel in the class I standard are much higher than those for surface water. In general, except for nickel, the infiltration fluid of all test soils conformed to the class II standard for groundwater (GB/T 14848-2017), that is, there was no impact on centralized drinking, industrial and agricultural production, breeding, etc. Therefore, based on the infiltration fluid content, SSL has the potential to be a green subgrade filler. In order to ensure full safety, edge wrapping can be incorporated with SL in the subgrade.

3.3.2. Permeability Test

Figure 13 shows the permeability coefficients of the test soils. The permeability coefficient of intact soil was 6.9×10^{-8} cm/s– 9.69×10^{-8} cm/s, and was within the range of the permeability coefficient of typical clay. For SSL, its permeability coefficient was much higher than that of intact soil, with a value of 4.25×10^{-4} cm/s– 1×10^{-2} cm/s, similar to the permeability coefficient of silty sand and medium sand. Therefore, SL can also be used as a permeable structure and material. Considering the potential trace elements of SL, a lower permeability coefficient means safety from dangerous elements. Therefore, silty clay and clay are often used for edge wrapping of contaminated subgrade filler. As shown in Figure 13, the addition of 50% SL increased the permeability coefficient of soil, and the test soil increased by 743%, consistent with the permeability coefficient range of clay and silty clay. Therefore, the permeability of potentially polluting elements can still be controlled; especially after adding 2% cement, the permeability coefficient of the test soil was close to 1.72×10^{-7} cm/s. In addition, the permeability coefficient of the test soils decreased with increasing compactness. For practical engineering applications, permeability can also be reduced by increasing compactness [34,35].

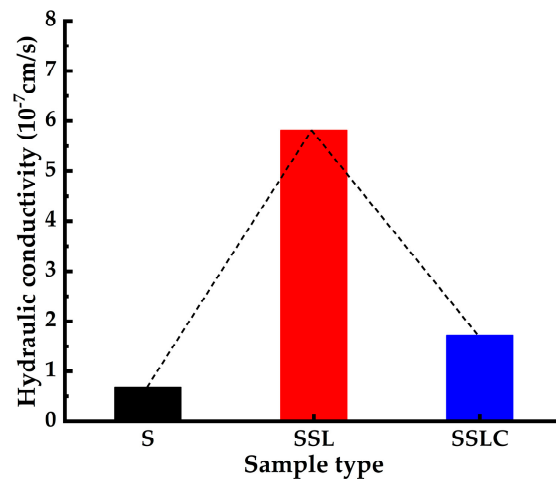


Figure 13. The permeability test results of the test soils.

4. Conclusions

In this study, the properties and effects of improved soil mixed with SL were evaluated based on physical and mechanical aspects and the environmental impact. The following conclusions were obtained:

(1) The conventional physical properties of intact soil were significantly affected by SL. Increased SL content led to increased maximum dry soil density, while optimum water content decreased. The liquid-plastic limit of SSL was lower than intact soil, and its plasticity index was also reduced.

(2) The addition of SL improved the CBR value of intact soil after 96 h-immersion. The CBR value of the improved soils increased first and then decreased, reaching the maximum CBR value of 60% at 50% SL, meeting the requirement for Class I expressway.

(3) Based on the compaction, Atterberg and CBR tests, the subgrade soil mixed with 50% SL had the highest CBR strength, good compaction characteristics and better stability. It also had the characteristics of a high utilization rate of SL.

(4) Strength parameters such as cohesion and friction angle of SSL under the optimal proportion significantly improved. The addition of cement further improved the soil strength.

(5) The dynamic modulus of the test soil improved by SL obviously increased, and the dynamic modulus of the test soil after adding cement was even more obvious, consistent with the static strength results.

(6) The pollution trace elements of SSL and SSLC were lower than that of SL, and could meet the class I standard of surface water and class II standard of ground water, which proves that SSL has the potential to be a green subgrade filler.

In conclusion, the physical and mechanical properties of SSL were better than intact soil, and the environmental pollution was low with no potential impact. The primary problem limiting the application of SL is its expansibility. In this paper, SL was used after aging for six months. Unlike other road structures, subgrade has stronger deformation compatibility, which is the focus of our subsequent studies.

Author Contributions: Conceptualization, Y.Z. and W.W.; Methodology, Y.Z. and T.J.; Validation, S.L.; Formal Analysis, T.J. and S.L.; Investigation, T.J. and S.L.; Writing-Original Draft Preparation, Y.Z.; Writing-Review and Editing, T.J., S.L. and W.W.; Project Administration, Y.Z. and W.W.; Funding Acquisition, Y.Z. and W.W. All authors have read and agreed to the published version of the manuscript.

Funding: This work was funded by the Science and Technology Base and Talent Special Project of Guangxi Province (grant number AD19245014), the Scientific and Technological Project of Science and Technology Department of Jilin Province (grant number: 20210508028RQ), National Natural Science Foundation of China (grant number: 52208438), and the Scientific Research Project of Department of Education of Jilin Province (grant number: JJKH20221019KJ).

Institutional Review Board Statement: Not applicable.

Informed Consent Statement: Not applicable.

Data Availability Statement: Not applicable.

Conflicts of Interest: The authors declare no conflict of interest.

References

1. Shu, K.; Sasaki, K. Occurrence of steel converter slag and its high value-added conversion for environmental restoration in China: A review. *J. Clean. Prod.* **2022**, *373*, 133876. [\[CrossRef\]](#)
2. Wang, X.; Li, X.; Yan, X.; Tu, C.; Yu, Z. Environmental risks for application of iron and steel slags in soils in China: A review. *Pedosphere* **2021**, *31*, 28–42. [\[CrossRef\]](#)
3. Guo, J.; Bao, Y.; Wang, M. Steel slag in China: Treatment, recycling, and management. *Waste Manag.* **2018**, *78*, 318–330. [\[CrossRef\]](#) [\[PubMed\]](#)
4. Shi, Y.; Chen, H.; Wang, J.; Feng, Q. Preliminary investigation on the pozzolanic activity of superfine steel slag. *Constr. Build. Mater.* **2015**, *82*, 227–234. [\[CrossRef\]](#)
5. Wang, K.; Qian, C.; Wang, R. The properties and mechanism of microbial mineralized steel slag bricks. *Constr. Build. Mater.* **2016**, *113*, 815–823. [\[CrossRef\]](#)
6. Wang, S.; Li, X.; Ren, K.; Liu, C. Experimental research on steel slag stabilized soil and its application in subgrade engineering. *Geotech. Geol. Eng.* **2020**, *38*, 4603–4615. [\[CrossRef\]](#)
7. Xu, P.; Zhang, D.; Miao, Y.; Sani, B.M.; Zhang, K. Development and characterization of a novel steel slag-based composite phase change aggregate for snow/ice melting of asphalt pavements. *Constr. Build. Mater.* **2022**, *341*, 127769. [\[CrossRef\]](#)
8. Xie, J.; Wu, S.; Zhang, L.; Xiao, Y.; Ding, W. Evaluation the deleterious potential and heating characteristics of basic oxygen furnace slag based on laboratory and in-place investigation during large-scale reutilization. *J. Clean. Prod.* **2016**, *133*, 78–87. [\[CrossRef\]](#)
9. Sorlini, S.; Sanzeni, A.; Rondi, L. Reuse of steel slag in bituminous paving mixtures. *J. Hazard. Mater.* **2012**, *209*, 84–91. [\[CrossRef\]](#)
10. Ahmedzade, P.; Sengoz, B. Evaluation of steel slag coarse aggregate in hot mix asphalt concrete. *J. Hazard. Mater.* **2009**, *165*, 300–305. [\[CrossRef\]](#)
11. Zhou, X.; Zhao, G.; Tighe, S.; Chen, M.; Wu, S.; Adhikari, S.; Gao, Y. Quantitative comparison of surface and interface adhesive properties of fine aggregate asphalt mixtures composed of basalt, steel slag, and andesite. *Constr. Build. Mater.* **2020**, *246*, 118507. [\[CrossRef\]](#)
12. Chen, Z.; Xie, J.; Xiao, Y.; Chen, J.; Wu, S. Characteristics of bonding behavior between basic oxygen furnace slag and asphalt binder. *Constr. Build. Mater.* **2014**, *64*, 60–66. [\[CrossRef\]](#)
13. Pasetto, M.; Baliello, A.; Giacomello, G.; Pasquini, E. Sustainable solutions for road pavements: A multi-scale characterization of warm mix asphalts containing steel slags. *J. Clean. Prod.* **2017**, *166*, 835–843. [\[CrossRef\]](#)
14. Yaghoubi, E.; Yaghoubi, M.; Guerrieri, M.; Sudarsanan, N. Improving expansive clay subgrades using recycled glass: Resilient modulus characteristics and pavement performance. *Constr. Build. Mater.* **2021**, *302*, 124384. [\[CrossRef\]](#)
15. Mirzababaei, M.; Miraftab, M.; Mohamed, M.; McMahan, P. Unconfined compression strength of reinforced clays with carpet waste fibers. *J. Geotech. Geoenviron.* **2013**, *139*, 483–493. [\[CrossRef\]](#)
16. Li, W.; Lang, L.; Lin, Z.; Wang, Z.; Zhang, F. Characteristics of dry shrinkage and temperature shrinkage of cement-stabilized steel slag. *Constr. Build. Mater.* **2017**, *134*, 540–548. [\[CrossRef\]](#)
17. Liu, J.; Yu, B.; Wang, Q. Application of steel slag in cement treated aggregate base course. *J. Clean. Prod.* **2020**, *269*, 121733. [\[CrossRef\]](#)
18. Li, Q.; Li, B.; Li, X.; He, Z.; Zhang, P. Microstructure of pretreated steel slag and its influence on mechanical properties of cement stabilized mixture. *Constr. Build. Mater.* **2022**, *317*, 125799. [\[CrossRef\]](#)
19. Gao, B.; Yang, C.; Zou, Y.; Wang, F.; Zhou, X.; Barbieri, D.M.; Wu, S. Compaction procedures and associated environmental impacts analysis for application of steel slag in road base layer. *Sustainability* **2021**, *13*, 4396. [\[CrossRef\]](#)
20. Yildirim, I.Z.; Prezzi, M. Subgrade stabilisation mixtures with eaf steel slag: An experimental study followed by field implementation. *Int. J. Pavement Eng.* **2022**, *23*, 1754–1767. [\[CrossRef\]](#)
21. Ma, Y.; Luo, Y.; Ma, H.; Zhou, X.; Luo, Z. Upcycling steel slag in producing eco-efficient iron-calcium phosphate cement. *J. Clean. Prod.* **2022**, *371*, 133688. [\[CrossRef\]](#)
22. Tian, E.; Liu, Y.; Cheng, X.; Zeng, W. Characteristics of pavement cement concrete incorporating steel slag powder. *Adv. Mater. Sci. Eng.* **2022**, *2022*, 6360301. [\[CrossRef\]](#)
23. Zhang, S.; Ghoul, Z.; Mucci, A.; Bahn, O.; Provencal, R.; Shao, Y. Production of cleaner high-strength cementing material using steel slag under elevated-temperature carbonation. *J. Clean. Prod.* **2022**, *342*, 130948. [\[CrossRef\]](#)

24. Gu, X.; Yu, B.; Dong, Q.; Deng, Y. Application of secondary steel slag in subgrade: Performance evaluation and enhancement. *J. Clean. Prod.* **2018**, *181*, 102–108. [[CrossRef](#)]
25. Aldeeky, H.; Al Hattamleh, O. Experimental study on the utilization of fine steel slag on stabilizing high plastic subgrade soil. *Adv. Civ. Eng.* **2017**, *2017*, 9230279. [[CrossRef](#)]
26. Kua, T.-A.; Arulrajah, A.; Horpibulsuk, S.; Du, Y.-J.; Shen, S.-L. Strength assessment of spent coffee grounds-geopolymer cement utilizing slag and fly ash precursors. *Constr. Build. Mater.* **2016**, *115*, 565–575. [[CrossRef](#)]
27. Wu, Y.; Qiao, X.; Yu, X.; Yu, J.; Deng, Y. Study on properties of expansive soil improved by steel slag powder and cement under freeze-thaw cycles. *KSCE J. Civ. Eng.* **2021**, *25*, 417–428. [[CrossRef](#)]
28. Cui, C.; Yu, C.; Zhao, J.; Zheng, J. Steel slag/precarbonated steel slag as a partial substitute for Portland cement: Effect on the mechanical properties and microstructure of stabilized soils. *KSCE J. Civ. Eng.* **2022**, *26*, 3803–3814. [[CrossRef](#)]
29. Wu, Y.; Shi, K.; Yu, J.; Han, T.; Li, D. Research on strength degradation of soil solidified by steel slag powder and cement in seawater erosion. *J. Mater. Civil Eng.* **2020**, *32*, 04020181. [[CrossRef](#)]
30. Wei, H.B.; Zhang, Y.P.; Cui, J.H.; Han, L.L.; Li, Z.Q. Engineering and environmental evaluation of silty clay modified by waste fly ash and oil shale ash as a road subgrade material. *Constr. Build. Mater.* **2019**, *196*, 204–213. [[CrossRef](#)]
31. Saglam, S.; Bakir, B.S. Cyclic response of saturated silts. *Soil Dyn. Earthq. Eng.* **2014**, *61–62*, 164–175. [[CrossRef](#)]
32. Zhang, E.; Wang, X.; Wang, W.; Wang, H. Mechanical properties, durability and leaching toxicity of cement-stabilized macadam incorporating reclaimed clay bricks as fine aggregate. *Sustainability* **2022**, *14*, 8432. [[CrossRef](#)]
33. Jiang, P.; Chen, Y.W.; Wang, W.S.; Yang, J.D.; Wang, H.Y.; Li, N.; Wang, W. Flexural behavior evaluation and energy dissipation mechanisms of modified iron tailings powder incorporating cement and fibers subjected to freeze-thaw cycles. *J. Clean. Prod.* **2022**, *351*, 131527. [[CrossRef](#)]
34. Nguyen, V.; Pineda, J.A.; Romero, E.; Sheng, D. Influence of soil microstructure on air permeability in compacted clay. *Geotechnique* **2021**, *71*, 373–391. [[CrossRef](#)]
35. Huang, X.; Horn, R.; Ren, T. Soil structure effects on deformation, pore water pressure, and consequences for air permeability during compaction and subsequent shearing. *Geoderma* **2022**, *406*, 115452. [[CrossRef](#)]

Disclaimer/Publisher’s Note: The statements, opinions and data contained in all publications are solely those of the individual author(s) and contributor(s) and not of MDPI and/or the editor(s). MDPI and/or the editor(s) disclaim responsibility for any injury to people or property resulting from any ideas, methods, instructions or products referred to in the content.